Journal of Applied Polymer Science

Effect of $CuBr_2$ salt treatment on the performance of nanocolloidal PPy:PSS multilayer thin film counter electrodes of dye-sensitized solar cells

S. Maruthamuthu,[1,2] J. Chandrasekaran,[3] D. Manoharan,[3] S. N. Karthick,[4] Hee-Je Kim[4]

[1]Research & Development Centre, Bharathiar University, Coimbatore, 641 046, Tamil Nadu, India
[2]Faculty of Physics, Dr. Mahalingam College of Engineering and Technology, Pollachi, 642 003, Tamil Nadu, India
[3]Department of Physics, Sri Ramakrishna Mission Vidyalaya College of Arts and Science, Coimbatore, 641 020, Tamil Nadu, India
[4]School of Electrical Engineering, Pusan National University, Busan, 609 735, Republic of Korea
Correspondence to: S. Maruthamuthu (E-mail: smaruthamuthu@gmail.com)

ABSTRACT: A thin Pt layer on fluorine-doped tin oxide (FTO) glass is commonly used as the counter electrode (CE) for dye-sensitized solar cells (DSCs). We have investigated thin layers on FTO glass made from spherical polypyrrole (PPy)–poly(styrene sulfonate) (PSS) nanocolloidal particles with and without treatment of $CuBr_2$ and used them as CEs. The colloidal polymer composite (PPy:PSS) was spin-coated at 4000 rpm, and PPy:PSS multilayer (one, three, five) films were employed as the CEs. Aqueous solutions of $CuBr_2$ (0.5 *M* and 1 *M*) were coated onto the multilayer CEs, which increased the efficiency of DSCs. When compared with the untreated PPy:PSS counter electrodes, the $CuBr_2$-treated PPy:PSS films showed lower charge-transfer resistance, higher surface roughness, and improved catalytic performance for the reduction of I_3^-. The enhanced catalytic performance is attributed to the interaction of the superior electrocatalytic activity of PPy:PSS and $CuBr_2$ salt. Under standard AM 1.5 sunlight illumination, the counter electrodes based on a single-layer PPy:PSS composite with 0.5 *M* and 1 *M* $CuBr_2$ salt treatment demonstrated power conversion efficiencies (PCE) of 5.8% and 5.6%, respectively. These values are significantly higher than that of the untreated PPy:PSS CE and are comparable with that of a Pt CE. © 2016 Wiley Periodicals, Inc. J. Appl. Polym. Sci. **2016**, *133*, 43772.

KEYWORDS: colloids; conducting polymers; films; nanostructured polymers; optical and photovoltaic applications

Received 13 January 2016; accepted 8 April 2016
DOI: 10.1002/app.43772

INTRODUCTION

The mass consumption and exhaustion of unsustainable energy sources have motivated modern researchers to design and utilize sustainable energy sources that do not rely on fossil fuels. Dye-sensitized solar cells (DSCs), a special type of photoelectron chemical solar cell, have been promising potential candidates for the production of electricity from solar energy in an efficient and ecofriendly manner.[1] Several novel materials have been employed as photoanode, electrolyte, dye, and counter electrode (CE) to improve the performance of DSCs.[2,3] The power-conversion efficiency of DSCs has exceeded 11%, which makes them promising for commercialization.[4,5] A counter electrode is a vital component in a DSC because it collects the electrons from the external circuit and allows the I_3^- reduction reaction. It acts as a mediator in regenerating the sensitizer after electron injection and serves to transfer electrons from the external circuit back to the redox electrolyte.[6] Typically, platinum (Pt) is employed as a CE because of its excellent electrocatalytic ability, chemical stability, and electrical conductivity.[7,8] However, Pt is a rather expensive metal, and platinum iodides such as PtI_4 or H_2PtI_6 will be generated when Pt is dissolved in solutions containing triiodide, which may affect the performance of DSCs.[9] Therefore, it is necessary to develop new Pt-free CEs with high stability and conductivity and efficient catalytic activity. However, a variety of CE materials have been exploited to date, based on metal compounds, polymers, carbon, composites, and multiple compounds. These materials showed relatively good catalytic performance for triiodide reduction to the Pt electrode, as was summarized by previous research.[10] Among them, conducting polymers are promising CE materials for DSCs. They are preferred because of their relatively low cost, high conductivity, large electrochemical surface area, and good electrocatalytic activity for I_3^- reduction.[11,12] Though poly(3,4-alkylenedioxythiophene) and polyaniline have been adopted as

Additional Supporting Information may be found in the online version of this article

CEs for DSCs, polypyrrole (PPy) is the most promising candidate, which exhibits significant versatility based on its particle size and is tunable in the presence of an anionic surfactant.[13–18] Though PPy receives considerable interest, processing it into an ultrathin film is a challenging task because of its intractability, insolubility, and infusibility in most common organic solvents.[19,20] PPy is usually synthesized by electrochemical and chemical oxidative polymerization techniques; in both processes they exhibit poor solubility.[21,22] By using a water-dispersible anionic polyelectrolyte, poly(styrene sulfonate) (PSS), as a charge-balancing dopant during the polymerization of pyrrole, the solubility problem can be circumvented. Interestingly, the solubility of PPy can be enhanced by designing colloidal forms using surfactants.[16,23] With the functional sulfonate groups, PSS will act as a structure-directing agent and will alter the morphology of PPy. The physical and chemical properties of PPy are considerably dependent upon the dopants and polymerization conditions.[14,15] Hence, PPy can be strategically tailored to form nanoscale thin films. Nanostructured PPy can provide better electron conduction pathways for rapid collection of photogenerated electrons.[24,25] Moreover, PPy is found to have more hydrophilic surface area when doped with PSS having free charges in its long strands. This could facilitate the enhanced conductivity and good electrocatalytic behavior of PPy.[26] A high concentration of PSS demonstrates a soft template effect with nanostructured PPy, having a highly ordered polymer chain structure.[27] Since the incorporation of PSS as dopant in PPy can significantly improve the properties of PPy, this motivated us to synthesize and employ nanocolloidal PPy:PSS thin films as CEs for DSCs. Though PPy was investigated as an alternative CE material for DSC, composites of PPy with metal nanostructures such as Pt, Au, Ag, Cu, and Pd receive research attention because of their unique optical and catalytic properties.[28–31]

In this article, we describe a rational approach for the construction of nanometer-sized spherical PPy:PSS colloidal particles. A core of a conducting polymer was formed via oxidative polymerization of a suitable monomer (pyrrole), which is surrounded by a corona of a polyelectrolyte PSS. In complexing PPy, the PSS chains attached to the PPy surface are not completely consumed. Rather, a sufficient fraction remains to electrosterically stabilize the individual colloidal particles. The PPy:PSS composite is believed to be a colloidal suspension in which there is a modifiable excess of PSS. This nanocolloidal suspension was spin-coated on fluorine-doped tin oxide (FTO) at 4000 rpm. With the aqueous dispersion of PPy:PSS we have designed thin and uniform multilayer (one, three, five) films. Although PPy thin films as CEs for DSCs have been studied, composites based on PSS and Cu have not yet been explored. The novelty of the present work is that the photovoltaic performance of DSCs using a PPy:PSS multilayer (one, three, five) CE was boosted through an aqueous solution of $CuBr_2$ salt treatment with different molarities (0.5 *M* and 1 *M*). The ion-induced charge screening developed by the $CuBr_2$ salt treatment replaced the excess PSS, with the anions from the salt as counterions of PPy. When compared to untreated films, the salt-treated multilayer PPy:PSS films exhibited conformational change of PPy chains and loss of some PSS, which improved their catalytic activity. The impact of bulky anions in the polymerization process and their effect on the PPy:PSS multilayer CEs is examined. The morphological variations and electrocatalytic behavior of multilayer films were analyzed relative to 0.5 *M* and 1 *M* $CuBr_2$ salt treatment. Finally, the incorporation of these $CuBr_2$ salt–treated PPy:PSS multilayer films as CEs is successfully shown to lead to improved power conversion efficiencies (PCE) because of an increase in the short-circuit current density (J_{sc}) and is comparable with conventional Pt CEs.

EXPERIMENTAL

Synthesis of PPy:PSS Nanocolloidal Spherical Particles

PPy:PSS spherical nanocolloidal particles were synthesized by an *in situ* chemical polymerization method. In a typical synthesis, 15 wt % of PSS (corresponds to monomer weight) was dissolved in 90 mL of distilled water in a reaction vessel containing 1 *M* aqueous HCl solution. Pyrrole (Py) monomer (0.67098 g) was added dropwise into the solution and continuously stirred for 30 min. In the presence of hydrochloric acid, Py monomers were protonated onto positively charged pyrrolinium ions and subsequently combined with negatively charged sulfonate groups of PSS in aqueous solution. The pyrrolinium ion–PSS complexes were formed by electrostatic interaction, and the polymerization of Py monomer proceeded by adding 2.28 g (10 mmol dissolved in 10 mL of distilled water) of ammonium peroxydisulfate [APS; $(NH_4)_2S_2O_8$] slowly into the solution containing monomer with HCl and PSS. With constant mechanical stirring of the solution, the polymerization was carried out for 24 h at 5 °C. Stable black-colored PPy:PSS nanocolloidal particles were obtained that were not precipitated because of a strong electrostatic interaction between PPy and PSS, and they are well dispersed in aqueous solution. The chemical structure of the polymer used is shown in Scheme 1.

Preparation of Multilayer PPy:PSS Composite Thin-Film Counter Electrodes

PPy:PSS composite films were prepared by spin-coating the nanocolloidal PPy:PSS aqueous solution on a fluorine-doped tin oxide (FTO) glass substrate with sheet resistance 13 Ω/sq, (Hartford Glass Co., Hartford City, Indiana, USA). All the substrates were precleaned with detergent, deionized (DI) water, acetone, and isopropyl alcohol in sequence and preheated at 90 °C for 3 min. After cooling the FTO to room temperature, the PPy:PSS nanocolloidal solution was then spin-coated at 4000 rpm for 30 s, and multilayer (one, three, five) films were prepared. After each single layer coating, the substrate was heated at 120 °C for 3 min and cooled to room temperature. Likewise, one-, three-, and five-layered films were prepared. Then all the films were dried at 120 °C for 30 min. For all the PPy:PSS multilayer films, a 150 μL aqueous solution of 0.5 *M* and 1 *M* $CuBr_2$ (Sigma-Aldrich 99% purity, Bengaluru, India) was spin-coated separately, and all the films are post-heated at 140 °C for 5 min. The salt-treated PPy:PSS multilayer films were cooled to room temperature in air and rinsed with deionized water, and finally the films were dried in a vacuum oven at 140 °C for 30 min. Similarly, PPy:PSS multilayer films without salt treatment were also prepared by the same procedure. A

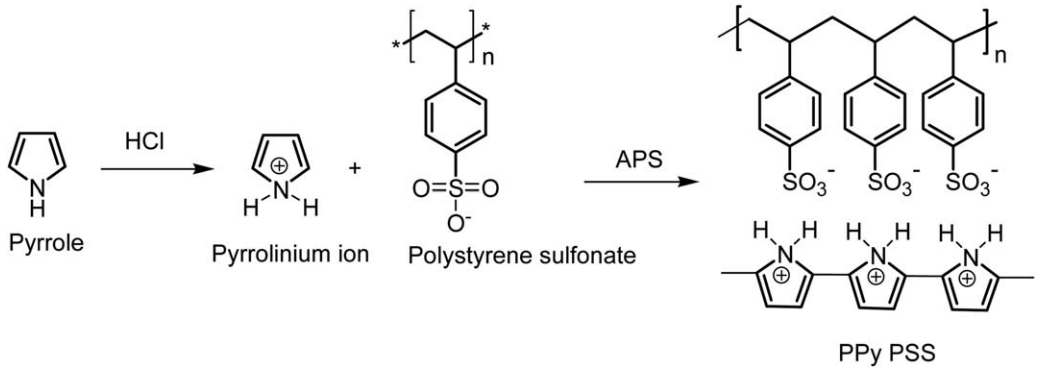

Scheme 1. Chemical structure of PPy:PSS.

counter electrode with an active area of 0.25 cm^2 is used for the DSC fabrication.

Fabrication of DSCs Based on PPy:PSS CE

To prepare the DSC, an FTO glass (Hartford Glass Co.), which was used as a current collector with a resistance of 13 Ω/sq was first cleaned for 10 min each in acetone, ethanol, and water through an ultrasonic bath. Adhesive tape was used as a spacer to control the film thickness, and it also created a noncoating area for electrical contact. TiO_2 (Ti-Nano oxide T/Sp, Solaronix, Aubonne, Switzerland) paste was coated on an FTO plate by the doctor-blade method and was used as the photoanode. The films thus coated were air-dried for 5 min to reduce the surface irregularities of TiO_2. To remove the organic loads, the films were annealed at 450 °C in air for 30 min, which facilitated the interconnection of TiO_2 nanoparticles. The photoanode thus prepared had a thickness of 20 μm with an active area of 0.20 cm^2. After cooling down to 75 °C, the TiO_2 film electrodes were immersed in a 0.3 m*M* N719 dye solution for 24 h. After dye adsorption, the film was rinsed with pure ethanol to remove the excess dye and dried with hot air. The Pt electrode was prepared from Pt paste (Plastisol T/sp, Solaronix) by the doctor-blade method. After coating on an FTO plate, it was annealed at 450 °C for 30 min. The dye-covered TiO_2 photoanode and 0.5 *M* and 1 *M* $CuBr_2$ treated multilayer PPy:PSS counter electrodes along with untreated PPy:PSS CEs were separately assembled as a sandwich type using a thermoplastic hot-melt ionomer film (SX 1170, Solaronix). The active cell area used was 0.25 cm^2. A drop of an Iodolyte AN-50 electrolyte solution (purchased from Solaronix) was injected into the cell through a hole at the back of the CE. The hole was covered with a cover glass on a hot-melt ionomer film and then sealed. Finally, the edge of each side of the FTO glass was cleaned and soldered (Ultrasonic soldering system Model-9200, Switzerland) with alloy #143 (Cerasolza, Switzerland) to achieve good electrical contact for the measurements.

Characterization Techniques

To obtain the solid form of PPy:PSS nanoparticles, the water-dispersible PPy:PSS nanoparticles were precipitated with an excess of ethanol. The precipitated particles were dried at 60 °C in vacuum for 24 h. A Fourier transform infrared (FTIR) spectrum of the sample in a KBr pellet was obtained using a (Bruker, Ettlingen, Germany, IFS 66 V, and (IRAffinity-1 Shimadzu, Japan) IR spectrophotometer. The surface morphology of the PPy:PSS nanoparticles was characterized using transmission electron microscopy (JEOL JEM 2100, Japan). The surface roughness and topology of the 0.5 *M* and 1 *M* $CuBr_2$ treated PPy:PSS multilayer films along with the untreated PPy:PSS CE films were analyzed by atomic force microscopy (AFM; model Solver Pro M of NT-MDT working in semicontact mode, Berlin, Germany). The particle size distribution of the PPy:PSS colloidal solution was determined by laser light scattering with a (Zetasizer) particle size analyzer (Malvern, UK). Cyclic voltammetry (CV) measurements were carried out on a CHI 660 C electrochemical workstation (CH Instruments, Austin, USA) using a three-electrode system with untreated PPy:PSS multilayer films and 0.5 *M* and 1 *M* $CuBr_2$ treated PPy:PSS multilayer films having an area of 1 × 1 cm^2 as working electrodes, Pt wire as CE, and an Ag/AgCl as reference electrode dipped in 0.1 *M* H_2SO_4 electrolyte solution in the range of −0.2 to 1 V at a scan rate of 50 mV s^{-1}. The electrochemical impedance spectroscopy (EIS) of salt-treated and untreated PPy:PSS multilayer counter electrodes was investigated by using a BioLogic potentiostat/galvanostat/EIS analyzer (SP-150, Claix, France) at room temperature in the frequency range of 1 mHz to 100 kHz with an AC amplitude of 10 mV under AM 1.5 sun illumination with a light intensity of 100 mW cm^{-2}. The current density–voltage (*J-V*) curves of the assembled DSCs were performed using a solar simulator (SAN-EI Electric XES-301 S 300W Xe lamp Kamishinjo, Higashi-Yodogawa, Osaka, Japan) under 1 sun illumination (AM 1.5G, 100 mW cm^{-2}). A Keithley, Beaverton, OR, USA 2400 was used as the source measurement unit.

RESULTS AND DISCUSSION

Formation of PPy:PSS Nanocolloidal Particles and Salt-Treatment Mechanism on Thin Films

The morphology of PPy is influenced by the concentration of Py monomer, (APS) oxidizing agent, and surfactant. PSS with 15 wt % will act as a counterion to PPy and also as a surfactant in the polymerization.[32] The amphiphilic nature of PSS in aqueous solutions will enable them to assemble into micelles of spherical structure. When the pyrrole monomer is added, because of its hydrophobic nature, they will penetrate into the

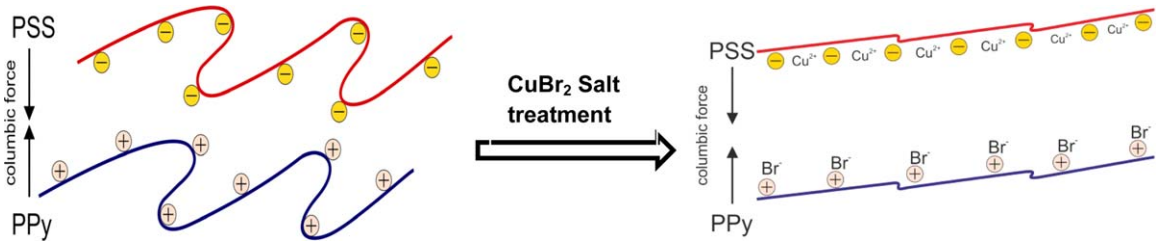

Scheme 2. Schematic representation of the conformational variation in PPy:PSS before and after $CuBr_2$ treatment. [Color figure can be viewed in the online issue, which is available at wileyonlinelibrary.com.]

interior of the micelle aggregation.[33] Subsequently, adding APS to the solution will gradually diffuse into pyrrole and oxopolymerize the pyrrole monomer into polymer inside the individual micelle core. Finally, as a consequence of the spatial constraint on the micelles, sphere-like PPy:PSS nanoparticles are obtained. These particles were well dispersed because of the higher concentration of PSS.

$CuBr_2$ treatment will bind the Cu^{2+} ions with the PSS anions, and the Cu^{2+} along with Br^- ions in the film will screen the charges on the PPy and PSS (Scheme 2). The positively charged PPy chains and negatively charged PSS chains of PPy:PSS can be considered as a polyelectrolyte complex. Hence, the $CuBr_2$ salt treatment will induce the charge screening and conformational change on the polyelectrolyte complexes.[34] Because of charge screening, the columbic attraction between PPy and PSS will be weakened. As a result, when a high concentration of $CuBr_2$ salt treatment was given, some of the PSS chains will leave the film, which is confirmed in the AFM analysis. Hence, the PPy conformational changes are the result of a weakening attraction between PPy and PSS and the expelling of PSS chains. The counterion can also play a role in controlling the ordering and orientation of the polymer and hence exploiting the assembly of the surfactant molecule.[35] The loss of excess insulating PSS and the conformational change of PPy could enhance the conductivity of the PPy:PSS films, which can improve the PCEs of multilayer films. Modification of the counterion using bromide could produce significant variations in the charge-transport properties and electron affinity in polymer solar cells leading to higher PCEs, which was also notably reported by Henson *et al.*[36] These findings indicate that modifying the nature of counterions in the CE of such polymer solar cells presents a promising approach for further improvement in device performance.

Structural and Morphological Analysis

The structural analysis of PPy:PSS was carried out by FTIR spectroscopy. Figure 1(a) shows the FTIR spectrum of the polymerized five-layer PPy:PSS films with and without salt treatment. The hydrated water molecules associating with the sulfonic acid groups (—SO_3H) via hydrogen bonding were revealed through a weak absorption band at 1640 cm^{-1}.[37] The strong peaks located at 1554 cm^{-1} and 1466 cm^{-1} are attributed to the characteristic asymmetric and symmetric stretching modes in the pyrrole ring, respectively. The broad bands at 788 cm^{-1} and 1103 cm^{-1} are due to C—H vibration.[38] The strong peaks at 1209 cm^{-1} and 1314 cm^{-1} are attributed to N—O stretching and N—H deformation vibrations.[39] The incorporation of dopant ions into the grown polymer is confirmed by the band at 925 cm^{-1}, which is the indication of the doping state of PPy.[40] The low absorption band at 680 cm^{-1} is due to C—H out-of-plane bending of the pyrrole moiety in PPy, and the bands near 600 cm^{-1} are the S—O stretching modes of the sulfate ions.[41] The effective conjugate chain length of the PPy is the ratio of the integral intensity of absorption at 1554 cm^{-1} and 1466 cm^{-1}. Hence, the obtained PPy:PSS nanoparticles possess an effectively long conjugate chain length.

High-resolution (HR) TEM was used to analyze the morphology of polypyrrole, synthesized by *in situ* chemical oxidative polymerization in the presence of 15 wt % of PSS. The HR-TEM images of different magnification are shown in Figure 1(b,c,d). They reveal that the polypyrrole nanoparticles were

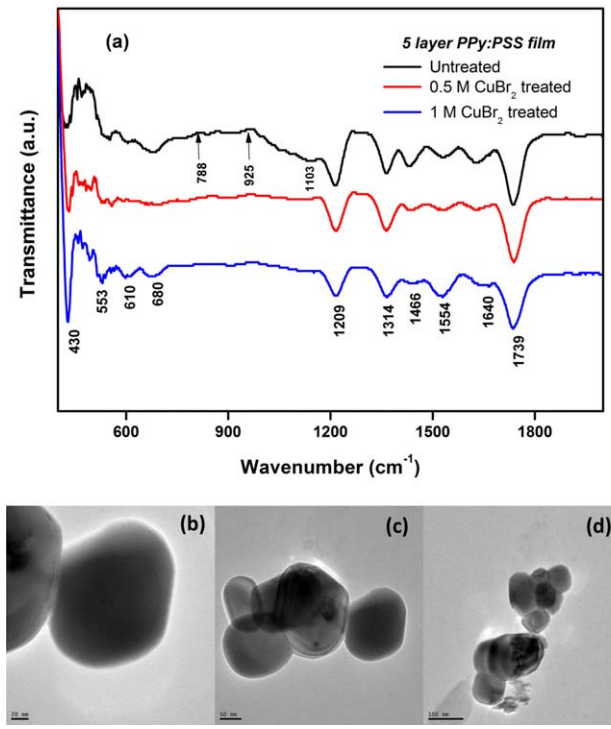

Figure 1. (a) FTIR spectrum of $CuBr_2$-treated and untreated five-layer PPy:PSS film and (b,c,d) TEM images of the synthesised PPy:PSS nanoparticles at different magnifications. [Color figure can be viewed in the online issue, which is available at wileyonlinelibrary.com.]

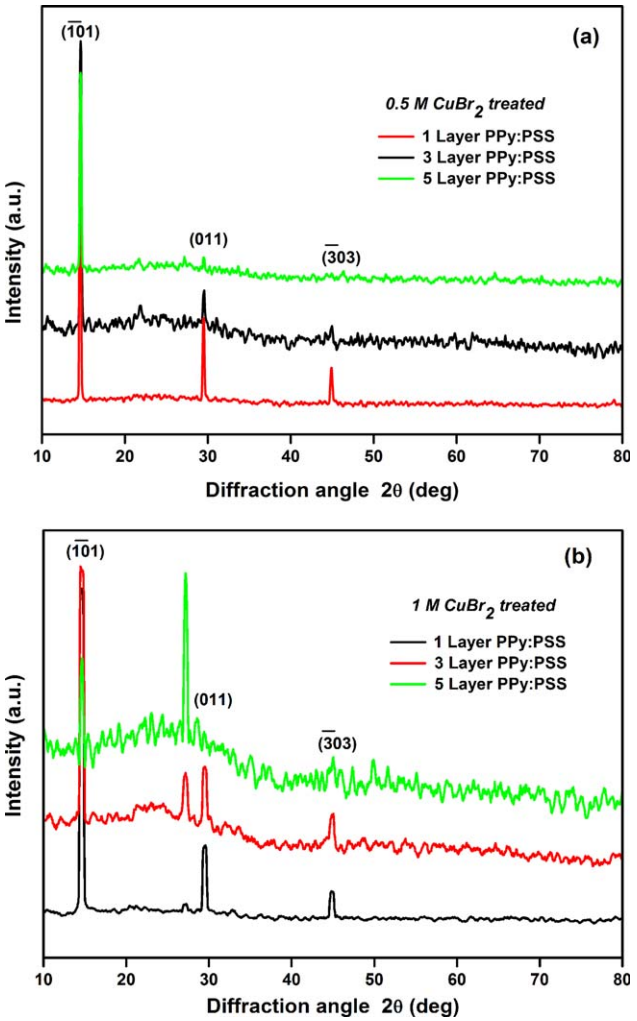

Figure 2. XRD spectra of PPy:PSS multilayer films treated with (a) 0.5 *M* $CuBr_2$; (b) 1 *M* $CuBr_2$. [Color figure can be viewed in the online issue, which is available at wileyonlinelibrary.com.]

very smooth and spherical in nature with an average diameter of 360 nm. The presence of a higher concentration of PSS acting as counterions for the PPy chain would disrupt the spherical micelles. Hence, spherical PPy particles of variable size were observed with the particle size analyzer, which is in accordance with the HR-TEM images. It is worth mentioning here that PPy:PSS nanoparticles were fabricated as individual discrete particles, which is very useful for their stable dispersion. During polymerization, the presence of bulky anions in the PPy matrix has a great impact on the microstructure and porosity of the PPy. The larger size of PSS will facilitate the PPy chain branching. When the PPy:PSS is spin-coated, the multilayer film would exhibit a porous structure with improved roughness, which was confirmed by the AFM results. Hence, the difference in PPy:PSS nanoparticle distribution when preparing multilayer films might significantly influence the electrocatalytic reactions, which is in accordance with the CV results obtained. Based on the above analysis, this variation in morphological characteristics of PPy is an indication that PPy nanoparticles were synthesized successfully via chemical oxidative polymerization within the surfactant micelles.

The X-ray diffraction (XRD) pattern of the PPy:PSS multilayer films treated with 0.5 *M* and 1 *M* $CuBr_2$ were analyzed, and the corresponding peaks are indexed using JCPDS Card No. 00-045-1063. The characteristic peaks at $2\theta = 14.4°$, 29.4°, and 44.3° represent the Bragg reflections from the $(\bar{1}00)$, (011), and $(\bar{3}03)$ planes of $CuBr_2$, respectively, confirming the presence of copper in the PPy:PSS composite. These sharp peaks indicate the crystalline behavior and the formation of an Face Centered Cubic structure of copper in the PPy:PSS composite. The salt-treated PPy:PSS films indicate the ordered polypyrrole chains, in which the intrachain and interchain hopping will be higher.[42] This means the carrier charge mobility will be higher, leading to an enhanced conductivity for salt-treated PPy:PSS composite films. Table S1 in the Supporting Information shows the calculated values of interchain separation (R), interplanar distance (d), and average particle size (L) for the $CuBr_2$-treated multilayer PPy:PSS composite films.[43] For salt-treated multilayer PPy:PSS composite films, the average particle size of the characteristic peak increased up to 14.04 nm, which is higher than untreated PPy:PSS (1.27 nm). Interestingly, the interchain separation decreased up to 2.52 Å after incorporation of $CuBr_2$ in the multilayer PPy:PSS surface, and it is less than in untreated films (4.65 Å). This clearly shows that the decoration of copper particles on the PPy surface is due to the formation of π-π coordination bonds.[44] During salt treatment, the interaction of PPy and $CuBr_2$ layers leads to a closely packed polymer chain. The enhanced degree of crystallinity with an increase in concentration of $CuBr_2$ is an indication that the structure of PPy is strongly influenced by the concentration of $CuBr_2$ and PSS. It is worth mentioning here that the sharp peaks are absent in untreated PPy:PSS films (see Figure S1 in the Supporting Information); rather there was a hump at $2\theta = 23.89°$ that is specifically due to conducting amorphous polypyrrole.[45] The peak corresponds to $d = 3.71$ Å, which is thought to arise from PPy chains. In the same region, for 0.5 *M* and 1 *M* $CuBr_2$ treated PPy:PSS films, there was a broad reflection that indicated the presence of PPy after a few PSS were removed due to the $CuBr_2$ salt treatment. The d spacings corresponding to the peaks $2\theta = 29.4°$ and 44.3° for salt-treated PPy:PSS film are 3.02 Å and 2.03 Å, respectively. When compared to untreated films this is lower, which may contribute more toward the conductivity by interchain hopping. The high-angle sharper peak at $2\theta = 29.4°$ for salt-treated films indicates the hierarchical polymer backbone. It reveals the more regular alignment and orientation of PPy:PSS molecular chains than of those in untreated films.[46] Hence, for salt-treated PPy:PSS films, a more homogeneous stress distribution can occur in the PPy matrix with a more ordered structure during oxidation and reduction, which would improve the electrocatalytic activity of these films. Interestingly, the intensity of the $2\theta = 29.4°$ peak was found to be reduced for salt-treated multilayer PPy:PSS films. This is because the insertion of excess SO_3^- groups in the PPy matrix will distort the structure of PPy molecules in multilayer films.[37] Hence, the decrease in the intensity of this peak is an indication of the removal of excess PSS due to $CuBr_2$ treatment. For the

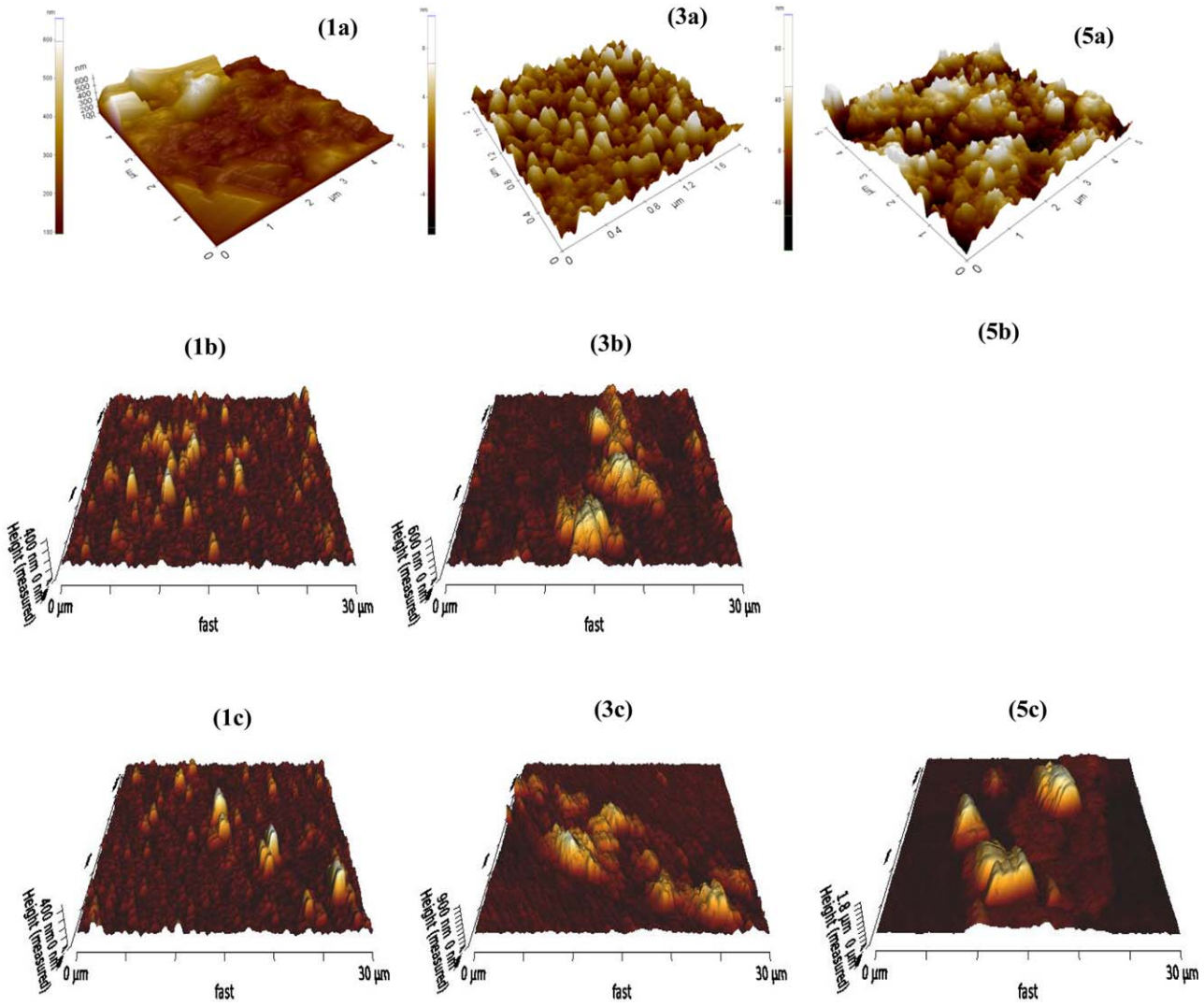

Figure 3. AFM images of PPy:PSS composite (one-, three-, and five-layer) films: 1a, 3a, and 5a are without $CuBr_2$ treatment; 1b, 3b, and 5b are 0.5 *M* $CuBr_2$ treated; and 1c, 3c, and 5c is 1 *M* $CuBr_2$ treated. [Color figure can be viewed in the online issue, which is available at wileyonlinelibrary.com.]

untreated films (Figure S1 in the Supporting Information), the broad peak at $2\theta = 26°$ corresponds to the face-to-face π-π stacking interaction of PPy chains, which is close to the interplanar van der Waals distance for aromatic groups.[45] The coulumbic attraction between the PPy and PSS is affected by the salt treatment, and the π-π interchain stacking distance is disturbed because they are spread on the entire surface of the film. Thus, for PPy:PSS multilayer (one, three, five) films treated with 0.5 *M* and 1 *M* $CuBr_2$, these peaks are suppressed because of the removal of a few excess PSS.

Figure 3 shows a distinctly different topography for untreated and $CuBr_2$ salt–treated PPy:PSS films. The rate of coverage for one-, three-, and five-layered, untreated and salt-treated samples were obtained based on the height exclusion from AFM images, which looks linear for multilayer films. This is an indication of the self-healing nature of PPy:PSS with respect to the addition of subsequent layers.[47] For untreated multilayer films as seen in Figure 3, the surface morphology shows many plate-like

Table I. AFM Parameters of Untreated and (0.5 *M* and 1 *M*) $CuBr_2$ Treated PPy:PSS Multilayer Films

Sample type	PPy:PSS layers	Roughness R_a (nm)	RMS R_q (nm)
Untreated PPy:PSS	1	18	30
	3	65.9	82.45
	5	89	109
PPy:PSS treated with 0.5 *M* $CuBr_2$	1	31.45	48.17
	3	71.11	98.90
	5	200.20	236.60
PPy:PSS treated with 1 *M* $CuBr_2$	1	32.13	51.10
	3	84.55	118.30
	5	232.40	345.60

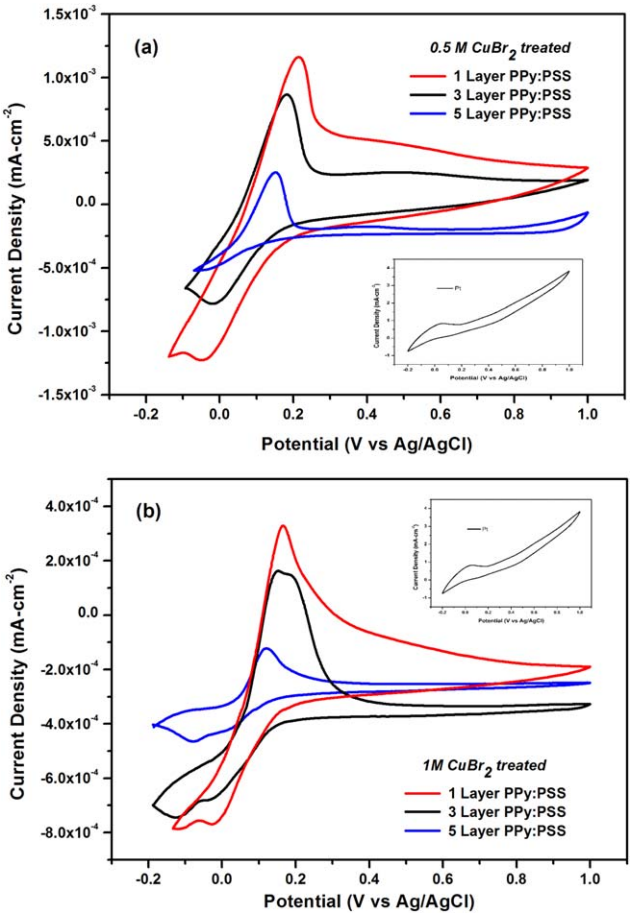

Figure 4. Cyclic voltammograms of PPy:PSS multilayer (one, three, five) films at a scan rate of 50 m V s^{-1} in 0.1 *M* H_2SO_4 aqueous solutions: (a) 0.5 *M* $CuBr_2$ treated films (b) 1 *M* $CuBr_2$ treated films (insert: Pt electrode). [Color figure can be viewed in the online issue, which is available at wileyonlinelibrary.com.]

particles or aggregates of particles covering the entire surface, respectively, thus having a relatively smaller surface roughness than $CuBr_2$-treated films, as shown in Table I. For 0.5 *M* and 1 *M* $CuBr_2$ treated PPy:PSS films, the surface morphology looks smooth with smaller domains. Interestingly, the average roughness of these PPy:PSS film surfaces improved up to 13.4 nm and 14.1 nm for a single layer when compared to untreated films. Similarly for three-layer PPy:PSS films with 0.5 *M* and 1 *M* salt treatment, the roughness was enhanced up to 5.2 nm and 18.6 nm, respectively. Likewise, for five-layer PPy:PSS films with 0.5 *M* and 1 *M* salt treatment, the roughness was increased up to 111 nm and 143 nm, respectively. These variations are due to the loss of some PSS chains during $CuBr_2$ treatment, which weakens the coulumbic attraction between PPy and PSS. Hence, the excess PSS in the films was removed by the salt treatment, and thus the plate-like aggregates of particles are affected and are spread as smaller domains over the entire surface, as seen in Figure 3. In multilayer PPy:PSS film formation, the thickness increment is the most straightforward parameter. There is a strong correlation between film thickness and surface potential at the PPy surface. With increasing film thickness, the surface potential on the PPy film would be reduced.[48,49] The thicker the PPy:PSS film, the rougher its surface will be. Hence, the multilayer PPy:PSS salt-treated films show enhanced roughness because of the increase in grain size (Table I). Increasing grain size can be attributed to the loss of a few PSS chains from PPy:PSS films. Moreover, the improved grain size can facilitate better charge transport across the grains.[50] The AFM results for PPy:PSS multilayer films indicate that the underlying film morphology constantly changes during spin-coating of PPy:PSS and $CuBr_2$ salt treatment. Thus, the PPy chains undergo conformational changes in the PPy:PSS films before and after salt treatment. The concentrations of $CuBr_2$ salt on PPy:PSS films have diverse effects on the conformation of the PPy chain. Significant changes could be seen in five-layer PPy:PSS films for 0.5 *M* and 1 *M* salt treated films, which show the larger R_{rms} value, which implies the largest electrocatalytic surface area for I_3^- reduction.[51] The evolution of PPy:PSS film roughness is consistent with the film growth behavior, which is due to the tendency of PPy:PSS polyelectrolyte to be a colloidal dispersion in aqueous medium.[52]

Electrochemical Analysis of PPy:PSS Multilayer Films

Cyclic voltammetry is the best tool to understand the electrocatalytic activity of $CuBr_2$ salt–treated and untreated PPy:PSS films. The CV curves of PPy:PSS multilayer films treated with 0.5 *M* and 1 *M* $CuBr_2$ are presented in Figure 4(a,b), respectively. The CV profile shows the well-defined oxidation and reduction peaks that confirm the better electrocatalytic activity of the electrodes. For untreated PPy:PSS films (Figure S2 in the Supporting Information), other than the single layer, these redox peaks look ill-defined. Interestingly for the 0.5 *M* and 1 *M* $CuBr_2$ treated single-layer PPy:PSS films, the cathodic peak current density improved up to 0.87×10^{-3} mA/cm^2 and 0.25×10^{-3} mA/cm^2, respectively. When compared to untreated films, these films demonstrated an enhanced electrocatalytic activity and better conductivity.[51] The same trend was also observed in AFM results with enhanced roughness, as shown in Table I. The ability of the electrode to reduce the triiodide ions is linearly related to the magnitude of the cathodic current density.[53] It is worth mentioning here that the enhanced current density is attributed to the hierarchical arrangement of PPy molecular chains after salt treatment for monolayer films, as confirmed in the XRD results. Evidently, relative to single-layer PPy:PSS films, when the number of bilayers of PPy:PSS was increased to three and five, the magnitude of the cathodic current density decreased. For 0.5 *M* and 1 *M* $CuBr_2$ treated multilayer films, the peak current densities were 0.1603×10^{-3} and 0.1182×10^{-3}, respectively, in which the former showed a higher value than the latter. For $CuBr_2$ salt–treated films, the presence of a greater number of active sites facilitates better electrocatalytic reactions. In multilayer PPy:PSS films, the lower magnitude of the cathodic current density harms the electrocatalytic activity. This is because, when the number of bilayers were increased to three and five, the thickness of the PPy:PSS film will increase, which will minimize the surface potential at the PPy surface. Thicker PPy:PSS films will have more roughness, which is supported by the AFM results. This leads to a lower probability of incorporation of Cu^{+2} and larger particle sizes for thin PPy:PSS films.[48,54] Hence, when the concentration of $CuBr_2$

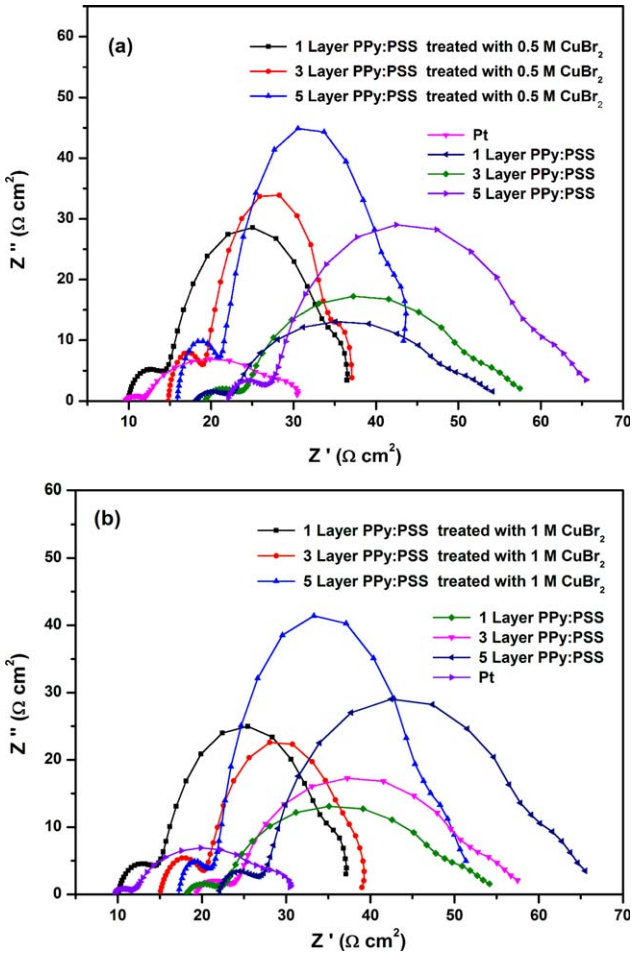

Figure 5. Nyquist plots of DSCs with PPy:PSS multilayer CEs, measured under a frequency of 0.01 Hz to 100 kHz: (a) 0.5 *M* $CuBr_2$ treated films compared with untreated films; (b) 1 *M* $CuBr_2$ treated films compared with untreated films. [Color figure can be viewed in the online issue, which is available at wileyonlinelibrary.com.]

is increased to 1 *M*, the observed trend is in accordance with an increase in the number of bilayers, which is related to the weak interactions of PPy and Cu^{+2} having a larger difference in surface potential between them.[49,55] Thus, we conclude that the higher concentration of $CuBr_2$ deposited on a multilayer PPy:PSS film surface would have a negative effect on the formation of a conductive path in PPy:PSS, resulting in low reduction ability for I_3^- to I^-. This trend might affect the power-conversion efficiency of the salt-treated multilayer films.

The electrochemical characteristics of PPy:PSS multilayer films treated with 0.5 *M* and 1 *M* $CuBr_2$ and untreated films were analyzed by electrochemical impedance spectroscopy (EIS). Figure 5(a,b) shows the Nyquist plots, which include high-frequency regions to low-frequency regions representing various resistances. At high frequency, the intersection of the semicircle at the real axis signifies the ohmic series resistance (R_s), representing the outside circuit resistance (substrate resistance and lead connections). The diameter of the high-frequency semicircle represents the charge transfer resistance (R_{ct}), corresponding to the electron transfer ability at the electrode/electrolyte interface. The low-frequency arc is attributed to the Nernst diffusion impedance (Z_w) of the triiodide/iodide redox couple in a thin layer of electrolyte.[56] The impedance parameters of PPy:PSS multilayer electrodes are summarized in Table II. It can be seen that the R_s values of PPy:PSS multilayer–based counter electrodes without $CuBr_2$ treatment vary between 17 and 21 Ω cm^2, which is higher than Pt. The larger R_s is attributed to the lower electrical conductivity.[57] For 0.5 *M* and 1 *M* $CuBr_2$ treated PPy:PSS multilayer films, because of the salt treatment, the R_s decreased significantly, as shown in Table II. This is attributed to the reduced thickness of the excess insulating PSS shell surrounding the conducting PPy grains due to salt treatment. We believe that $CuBr_2$ will induce segregation on a nanometer scale between PPy and excess PSS, allowing better pathways for conduction. Hence, smaller R_s values specify the possibility of improved electrical conductivity and firm bonding of the polymer composite with the substrate.[58] It is well established that R_{ct} is the most important part to demonstrate the catalytic ability of the counter electrodes. For 0.5 *M* $CuBr_2$ treated PPy:PSS multilayer films, R_{ct} was 4.5 Ω cm^2, 5.13 Ω cm^2, and 5.5 Ω cm^2, respectively for one-, three-, and five-layer films, which is apparently lower than untreated films but relatively higher than Pt. These results indicate that a lower interfacial charge-transfer

Table II. EIS Parameters for Untreated and (0.5 *M* and 1 *M*) $CuBr_2$ Treated PPy:PSS Multilayer Films and Pt Electrode

Sample type	PPy:PSS layers	R_s (Ω cm^2)	R_{ct1} (Ω cm^2)	R_{ct2} (Ω cm^2)
Untreated PPy:PSS	1	17.4	5.39	31.83
	3	18.70	5.68	34.23
	5	21.5	6.28	43.75
PPy:PSS treated with 0.5 *M* $CuBr_2$	1	9.82	4.51	20.14
	3	14.79	5.13	22.68
	5	15.84	5.5	23.20
PPy:PSS treated with 1 *M* $CuBr_2$	1	10.46	4.62	22.52
	3	15.06	5.27	28.67
	5	17.43	5.65	29.88
Pt	1	9.50	2.14	15.65

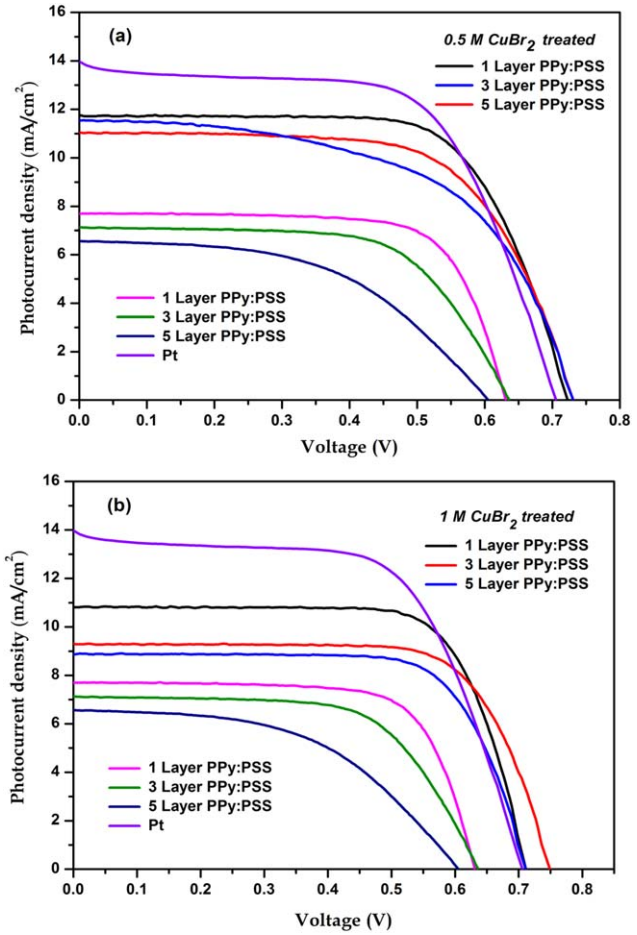

Figure 6. Current density–voltage (*J-V*) curves of DSCs based on PPy:PSS multilayer (one, three, five) films and Pt counter electrodes treated under AM 1.5 (100 m W cm^{-2}): (a) 0.5 *M* $CuBr_2$ treated films along with untreated films; (b) 1 *M* $CuBr_2$ treated films along with untreated films. [Color figure can be viewed in the online issue, which is available at wileyonlinelibrary.com.]

resistance occurred at the interface between the PPy:PSS $CuBr_2$ salt–treated CE and the electrolyte that is due to the enhanced electrical conductivity and improved electrocatalytic activity of the PPy:PSS film. This means that in salt-treated films the addition of Cu^{2+} in the PPy matrix minimized the R_{ct} of multilayered PPy:PSS counter electrodes. After a few PSS were replaced, the Cu^{2+} ions in the PPy matrix render a better contact among the polymer and I_3^- electrolytes. Hence, the efficient reduction reaction in the I_3^-/I^- system could enhance the catalytic activity, which is in accordance with the CV result. Interestingly, when the concentration of $CuBr_2$ is increased to 1 *M*, the R_{ct} obtained for the PPy:PSS multilayer (one, three, and five) films were 4.6 Ω cm^2, 5.17 Ω cm^2, and 5.65 Ω cm^2, respectively, which is relatively higher than Pt. Though this result is better than untreated films, these values are fractionally higher than 0.5 *M* $CuBr_2$ treated PPy:PSS films. One possible reason is that a higher wt % of PSS not only dispersed in the PPy matrix but also tends to aggregate on the surface of PPy.[52] Hence, during 1 *M* $CuBr_2$ salt treatment, more Cu^{2+} ions will be attached to the PPy matrix along with PSS, which would be a hindrance for the contact between the PPy matrix and the I_3^- electrolyte. Chen *et al.* notably reported[37] that the excess PSS with SO_3^- groups in the PPy matrix would cause a high degree of distortion in the conjugated PPy segments as a result of steric congestion. Moreover, the R_{ct2} corresponds to the charge-transfer process occurring at the TiO_2/dye/electrolyte interface. The large resistance is attributed to a certain perturbation in electrolyte diffusion, which might have greatly infused the impedance behavior in this region.

Photovoltaic Performance of DSC Based on PPy:PSS Multilayer Films

The photocurrent density–voltage (*J–V*) curves of the DSCs based on the PPy:PSS composite and 0.5 *M* and 1 *M* $CuBr_2$ treated multilayer PPy:PSS along with Pt counter electrodes are shown in Figure 6(a,b). The photovoltaic parameters of the DSCs are summarized in Table III. Among the different PPy:PSS composite CEs, the DSC with a 0.5 *M* $CuBr_2$ treated single layer exhibits a short-circuit current density (J_{sc}) of 11.7 mA cm^{-2}, an open-circuit voltage (V_{oc}) of 723 mV, and a fill factor (FF) of 0.648, yielding a power conversion efficiency (η) of 5.79%. These values are significantly higher than DSC employing untreated PPy:PSS composite (3.48%) and are comparable with

Table III. Photovoltaic Parameters of the DSCs Based on Untreated and (0.5 *M* and 1 *M*) $CuBr_2$ Treated PPy:PSS Multilayer Films as Counter Electrodes along with Pt CE under AM 1.5 (100 mW cm^{-2})

Counter electrode	PPy:PSS layers	J_{sc} (mA cm^{-2})	V_{oc} (V)	FF	η (%)
PPy:PSS	1	7.22	0.663	0.715	3.48
	3	7.12	0.635	0.639	2.90
	5	6.56	0.604	0.505	2.01
PPy:PSS treated with 0.5 *M* $CuBr_2$	1	11.76	0.723	0.648	5.79
	3	11.59	0.731	0.622	5.23
	5	11.05	0.730	0.562	4.76
PPy:PSS treated with 1 *M* $CuBr_2$	1	10.85	0.712	0.726	5.61
	3	9.31	0.749	0.716	5.00
	5	8.92	0.711	0.718	4.55
Pt	1	13.77	0.705	0.630	6.15

Pt CEs. In addition, PPy:PSS multilayer (three and five) films with 0.5 *M* $CuBr_2$ salt treated counter electrode films reached conversion efficiencies of 5.2% and 4.7%, respectively, which is greater than for untreated PPy:PSS composites (2.9% and 2.01%, respectively). This enhanced conversion efficiency was caused by the larger surface area created through incorporation of Cu^{2+}, leading to an improved electrolyte/electrode interaction.[59] The additional electrocatalytic sites induced by the $CuBr_2$ salt treatment could be beneficial for a faster rate of the I_3^-/I^- redox reaction on the electrode.[59] This is consistent with the improved J_{sc} of $CuBr_2$ salt–treated PPy:PSS CEs (Table III), which is due to the improved apparent catalytic activity for the reduction of I_3^-. This in turn controls the actual driving force for dye regeneration and is in good agreement with CV and AFM measurements.[60] These J_{sc} values are comparable with Pt CEs. Comparing the photovoltaic parameters of $CuBr_2$ salt–treated multilayer PPy:PSS counter electrodes and untreated CEs, it is observed that the untreated PPy:PSS films show much lower short-circuit current density (J_{sc}). The lower J_{sc} values of the untreated PPy:PSS composite films are consistent with the poor electrocatalytic activity of these films and is in accordance with the CV results. Also, the presence of an excess amount of bulky and hydrophobic anionic PSS surfactant affected the electrocatalytic activity and created higher charge-transfer resistance (R_{ct}), leading to relatively poor performance.[52] This is in accordance with the obtained EIS results. Thus, with $CuBr_2$ treatment on multilayer PPy:PSS films, we were able to demonstrate that the R_{ct} can be altered in the electrolyte/electrode interface. $CuBr_2$ salt treatment reduced the diffusion impedance of triiodide ions, which enhanced the J_{sc} of multilayer PPy:PSS CE films. Also, the smaller R_{ct} of 0.5 *M* salt treated PPy:PSS films have a facial electron movement toward the CE surface. This is attributed to the binding of Cu^{2+} metal ions to PSS anions, which is vital for the enhanced conductivity of PPy:PSS composite films. The metal ion Cu^{2+} with a positive softness parameter can strongly bind to PSS.[61] Consequently, some of the excess PSS anions would be replaced by Br^- ions as counterions for PPy. Thus the PPy:PSS multilayer films with incorporated Cu^{2+} ensured effective charge transfer at the CE–electrolyte interface, with a lower recombination rate in the DSC, which ultimately increased the power-conversion efficiency. Interestingly, as the concentration of $CuBr_2$ increased to 1 *M*, the multilayer (one, three, and five) PPy:PSS counter electrodes showed a fractional decline in the power-conversion efficiency of DSC (5.6%, 4.99%, and 4.53%, respectively) when compared to 0.5 *M* $CuBr_2$ treated multilayer films. One possible reason is the excess polyelectrolyte chain that is situated at the surface of PPy would collapse upon addition of multivalent counterions during a high-concentration $CuBr_2$ salt treatment (1 *M*). As a consequence, the PPy might form clusters in the excess PSS because of the incompatibility of the two polymers. Therefore, PPy-rich and PPy-poor microdomains will be formed in the excess PSS shell, which is consistent with the observations reported by Jianjun et al.[62] Also, the greater number of Cu^{2+} ions could be a barrier to contacts between an efficient PPy network and I_3^-. This may reduce the electron transport on the CE and the regeneration rates of dye molecules, which is in accordance with the CV results. The second reason might be the interaction between $(NH_4)_2S_2O_8$ and the surfactant PPy doped with sulfonate. Even though the dissociation of the anionic surfactant is prevented by the strongly electrolytic oxidant, the undissociated molecules of surfactant will appear to be thickly absorbed on the PPy surface, which may act as a steric stabilizer.[63] The presence of excess steric stabilizer might affect the conductivity of PPy.[64] These factors may lead to the reduced J_{sc} for multilayer PPy:PSS films treated with 1 *M* $CuBr_2$. Despite the relatively improved efficiency of 0.5 *M* and 1 *M* salt treated PPy:PSS counter electrodes, they are still less efficient than Pt-based DSCs. This is because the higher internal resistance of PPy:PSS-based untreated and salt-treated films leads to a reduced J_{sc} when compared to Pt. Furthermore, the photoreflection properties related to the PPy:PSS CEs, along with the greater photoabsorption ability of PPy:PSS materials, might be one of the factors.[65] It is worth mentioning here that in either case the DSC performance based on 0.5 *M* and 1 *M* $CuBr_2$ treated PPy:PSS counter electrodes is better than untreated PPy:PSS CEs. This is due to the salt treatment mechanism, which indicated the loss of excess PSS in the polymer films, along with the conformational change of PPy chains, which is in accordance with the AFM results. Interestingly, for the salt-treated PPy:PSS samples, the V_{oc} did not change drastically and looks similar, indicating that the value of V_{oc} is not affected by the molar ratio of $CuBr_2$.

CONCLUSIONS

Spherical PPy:PSS nanocolloidal particles have been successfully fabricated by a chemical oxidation process. PPy:PSS multilayer (one, three, and five) films were prepared by spin-coating the colloidal dispersion solution at 4000 rpm on an FTO glass plate and were deployed as CEs for dye-sensitized solar cells. Aqueous solutions of 0.5 *M* and 1 *M* $CuBr_2$ were applied on the PPy:PSS multilayer films, by which the charge-transfer resistance decreased up to ~12%. It has been demonstrated that single-layer PPy:PSS films with 0.5 *M* and 1 *M* $CuBr_2$ salt treatment present good catalytic activity for the I_3^- reduction. The DSCs based on the single-layer PPy:PSS with 0.5 *M* and 1 *M* $CuBr_2$ treated CEs reached a power-conversion efficiency of 5.8% and 5.6%, respectively, which is significantly higher than untreated PPy:PSS films (3.48%) and is comparable with that of Pt. This is attributed to the increase in the active surface area of PPy:PSS CEs due to $CuBr_2$ salt treatment, which could promote superior electrocatalytic activity for the I_3^- reduction and enhanced electrical conductivity for the I_3^-/I^- redox reaction, resulting in improved J_{sc} values (11.76 and 10.85 mA cm^{-2}) of DSC. Also, $CuBr_2$ salt treatment induced the conformational change of PPy, along with the charge-screening effect on the PPy:PSS multilayer film. Furthermore, the excess of bulky and hydrophobic anionic PSS surfactant, which affected the electrocatalytic activity in untreated films, was removed by salt treatment. Given the vast tunability offered by PPy, coupled with their solution processability, it can be expected that salt-treated PPy:PSS CE films will have a key role in improving the PCE of DSCs.

REFERENCES

1. Sara, T.; Deepak, T. G.; Anjusree, G. S.; Arun, T. A.; Naira, S. V.; Sreekumaran Nair, A. *J. Mater. Chem. A* **2014**, *2*, 4474.
2. Vijayakumar, E.; Vignesh, M.; Subramania, A.; Zhaofu, F.; Dyson, P. J. *J. Appl. Polym. Sci.* **2015**, *132*, DOI: 10.1002/app.42777.
3. Vijayakumar, E.; Pratheep, P.; Sivasankar, N.; Karthick, S. N.; Subramania, A. *Appl. Phys. A* **2015**, *120*, 1211.
4. Mohammad, K. N.; Angelis, F. D.; Fantacci, S.; Selloni, A.; Viscardi, G.; Liska, P.; Ito, S.; Takeru, B.; Gratzel, M. *J. Am. Chem. Soc.* **2005**, *127*, 16835.
5. Vijayakumar, E.; Subramania, A.; Fei, Z.; Dyson, P. J. *RSC Adv.* **2015**, *5*, 52026.
6. Vijayakumar, E.; Subramania, A.; Fei, Z.; Dyson, P. J. *J. Appl. Polym. Sci.* **2015**, *132*, DOI: 10.1002/app.42032.
7. Tai, S. Y.; Chang, C. F.; Liu, W. C.; Liao, J. H.; Lin, J. Y. *Electrochim. Acta* **2013**, *107*, 66.
8. Huo, J.; Wu, J.; Zheng, M.; Tu, Y.; Lan, Z. *J. Power Sources* **2016**, *304*, 266.
9. Olsena, E.; Hagen, G.; Lindquistc, S. E. *Sol. Energy Mater. Sol. Cells* **2000**, *63*, 267.
10. Wu, M.; Ma, T. *J. Phys. Chem. C* **2014**, *118*, 16727.
11. Ahmad, S.; Yum, J. H.; Xianxi, Z.; Gratzel, M.; Butt, H. J.; Nazeeruddin, M. K. *J. Mater. Chem.* **2010**, *20*, 1654.
12. Ahmad, S.; Yum, J. H.; Butt, H. J.; Nazeeruddin, M. K.; Gratzel, M. *Chem. Phys. Chem.* **2010**, *11*, 2814.
13. Jeon, S. S.; Kim, C.; Ko, J.; Im, S. S. *J. Mater. Chem.* **2011**, *21*, 8146.
14. He, B.; Tang, Q.; Liang, T.; Li, Q. *J. Mater. Chem. A* **2014**, *2*, 3119.
15. Xiao, Y.; Lin, J. Y.; Wang, W. Y.; Tai, S. Y.; Yue, G.; Wu, J. *Electrochim. Acta* **2013**, *90*, 468.
16. Xia, J.; Masaki, N.; Jiang, K.; Yanagida, S. *J. Mater. Chem.* **2007**, *17*, 2845
17. Yan, X.; Zhang, L. *J. Appl. Electrochem.* **2013**, *43*, 605.
18. Sun, H.; Luo, Y.; Zhang, Y.; Li, D.; Yu, Z.; Li, K.; Meng, Q. *J. Phys. Chem. C* **2010**, *114*, 11673.
19. Ram, M. K.; Salerno, M.; Adami, M.; Faraci, P.; Nicolini, C. *Langmuir* **1999**, *15*, 1252.
20. Cheung, J. H.; Stockton, W. B.; Rubner, M. F. *Macromolecules* **1997**, *30*, 2712.
21. Hong, H.; Davidov, D.; Chayet, H.; Avny, Y.; Faraggi, E. Z.; Neumann, R. *Adv. Mater.* **1995**, *7*, 846.
22. Zang, J.; Li, C. M.; Bao, S. J.; Cui, X.; Bao, Q.; Sun, C. Q. *Macromolecules* **2008**, *41*, 7053.
23. Stejskal, J. *J. Polym. Mater.* **2001**, *18*, 225.
24. Wu, J.; Li, Q.; Fan, L.; Lan, Z.; Li, P.; Lin, J.; Hao, S. *J. Power. Sources* **2008**, *181*, 172.
25. Zhong, W.; Liu, S.; Chen, X.; Wang, Y.; Yang, W. *Macromolecules* **2006**, *39*, 3224.
26. Fonner, J. M.; Forciniti, L.; Nguyen, H.; Byrne, J. D.; Kou, Y. F.; Nawaz, J. S.; Schmidt, C. E. *Biomed. Mater.* **2008**, *3*, 034124.
27. Wang, Y.; Gai, S.; Niu, N.; He, F.; Yang, P. *Phys. Chem. Chem. Phys.* **2013**, *15*, 16795.
28. Jiwei, L.; Jingxia, Q.; Miao, Y.; Chen, J. *J. Mater. Sci.* **2008**, *43*, 6285.
29. Feng, X.; Huang, H.; Ye, Q.; Zhu, J. J.; Hou, W. *J. Phys. Chem. C* **2007**, *111*, 8463.
30. Ding, K.; Jia, H.; Wei, S.; Guo, Z. *Ind. Eng. Chem. Res.* **2011**, *50*, 7077.
31. Rau, J. R.; Lee, J. C.; Chen, S. C. *Synth. Met.* **1996**, *79*, 69.
32. Wu, T. M.; Chang, H. L.; Lin, Y. W. *Polym. Int.* **2009**, *58*, 1065.
33. Goren, M.; Lennox, R. B. *Nano Lett.* **2001**, *1*, 735.
34. Chen, J. H.; Heitmann, J. A.; Hubbe, M. A. *Colloids Surf. A* **2003**, *223*, 215.
35. Chen, L.; Xie, C.; Chen, Y. *Macromolecules* **2014**, *47*, 1623.
36. Henson, Z. B.; Zhang, Y.; Nguyen, T. Q.; Seo, J. H.; Bazan, G. C.; *J. Am. Chem. Soc.* **2013**, *135*, 4163.
37. Chen, N.; Hong, L. *Eur. Polym. J.* **2001**, *37*, 1027.
38. Goel, S.; Mazumdar, N. A.; Gupta, A. *Polym. Adv. Technol.* **2010**, *21*, 205.
39. Jeon, S. S.; Park, J. K.; Yoon, C. S.; Im, S. S. *Langmuir* **2009**, *25*, 11420.
40. Wei, M.; Lu, Y. *Synth. Met.* **2009**, *159*, 1061.
41. Xia, Y.; Sun, K.; Ouyang, J. *Adv. Mater.* **2012**, *24*, 2436.
42. Bhadra, S.; Singha, N. K.; Khastgir, D. *J. Appl. Polym. Sci.* **2007**, *104*, 1900.
43. Ali, Y.; Kumar, V.; Sonkawade, R. G.; Dhaliwal, A. S. *Vacuum* **2013**, *90*, 59.
44. Ali, Y.; Sharma, K.; Kumar, V.; Sonkawade, R. G.; Dhaliwal, A. S. *Appl. Surf. Sci.* **2013**, *280*, 950.
45. Wang, J. P.; Xu, Y.; Wang, J.; Du, X.; Xiao, F.; Li, J. *Synth. Met.* **2010**, *160*, 1826.
46. Cheah, K.; Forsyth, M.; Truong, V. T. *Synth. Met.* **1999**, *101*, 19.
47. Paddeu, S.; Ram, M. K.; Carrara, S.; Nicolini, C. *Nanotechnology* **1998**, *9*, 228.
48. Singh, R.; Narula, A. K. *Synth. Met.* **1996**, *82*, 245.
49. Andreoli, E.; Liao, K. S.; Haldar, A.; Alley, N. J.; Curran, S. A. *Synth. Met.* **2013**, *185–186*, 71.
50. Xia, Y.; Ouyang, J. *Org. Electron.* **2010**, *11*, 1129.
51. Fan, M. S.; Chen, J. H.; Li, C. T.; Cheng, K. W.; Ho, K. C. *J. Mater. Chem. A* **2015**, *3*, 562.
52. Maruthamuthu, S.; Chandrasekaran, J.; Mahoharan, D.; Karthick, S. N.; Kim, H. J. *J. Appl. Polym. Sci.* **2016**, *133*, 43114.
53. Wu, M.; Lin, X.; Wang, Y.; Wang, L.; Guo, W.; Qi, D.; Peng, X.; Hagfeldt, A.; Gratzel, M.; Ma, T. *J. Am. Chem. Soc.* **2012**, *134*, 3419.
54. Pope, J. N.; Buttry, D. A. *J. Electroanal. Chem.* **2001**, *498*, 75.
55. Cole, D. H.; Shull, K. R.; Rehn, L. E.; Baldo, P. *Phys. Rev. Lett.* **1997**, *78*, 5006.

56. Cho, S. J.; Ouyang, J. *J. Phys. Chem. C* **2011**, *115*, 8519.

57. Joshi, P.; Zhang, L.; Chen, Q.; Galipeau, D.; Fong, H.; Qiao, Q. *ACS Appl. Mater. Interfaces* **2010**, *2*, 3572.

58. Wu, M.; Lin, X.; Wang, T.; Qiu, J.; Ma, T. *Energy Environ. Sci.* **2011**, *4*, 2308.

59. Aoyagi, M.; Funaoka, M. J. *Photochem. Photobiol. A* **2004**, *164*, 53.

60. Li, G. R.; Wang, F.; Jiang, Q. W.; Gao, X. P.; Shen, P. W. *Angew. Chem. Int. Ed.* **2010**, *122*, 3735.

61. Xia, Y.; Ouyang, J. *Macromolecules* **2009**, *42*, 4141.

62. Wang, J.; Sun, L.; Mpoukouvalas, K.; Lienkamp, K.; Lieberwirth, I.; Fassbender, B.; Bonaccurso, E.; Brunklaus, G.; Muehlebach, A.; Beierlein, T.; Tilch, R.; Butt, H. J.; Wegner, G. *Adv. Mater.* **2009**, *21*, 1137.

63. Kudoh, Y. *Synth. Met.* **1996**, *79*, 17.

64. Aldissi, M.; Armes, S. P. *Prog. Org. Coat.* **1991**, *19*, 21.

65. Ganapathy, V.; Karunagaran, B.; Rhee, S. W. *ACS Appl. Mater. Interfaces* **2011**, *3*, 857.

SGML and CITI Use Only
DO NOT PRINT